Investigation of particle-wall interaction in a pseudo-2D fluidized bed using CFD-DEM simulations

Tingwen Li[a,b*], Yongmin Zhang[c], Fernando Hernández-Jiménez[d]

[a] National Energy Technology Laboratory, Morgantown, WV 26507, USA
[b] AECOM, Morgantown, WV 26507, USA
[c] State Key Laboratory of Heavy Oil Processing, China University of Petroleum, Beijing 102249, China
[d] Universidad Carlos III of Madrid, Department of Thermal and Fluid Engineering, Av. de la Universidad, 30, 28911 Leganés, Madrid, Spain

Abstract

This paper reports discrete element method (DEM) simulations of a pseudo-two-dimensional (pseudo-2D) fluidized bed to investigate the particle-wall interaction. Detailed information on the macroscopic flow field variables including solids pressure, granular temperature, normal and tangential wall stresses are analyzed. It is found that the wall normal stress differs from the solids pressure due to the strong anisotropic flow behavior in the pseudo-2D system. There exists a simple linear relationship between the normal wall stress and the solids pressure. In addition, an effective friction coefficient can be derived for characterizing the particle-wall flow interaction after evaluating the normal and tangential wall stresses. The effect of inter-particle and particle-wall friction coefficient has been evaluated. The strong anisotropic flow behavior found in the pseudo-2D system should be considered for validation study of two fluid model (TFM) where the boundary condition is usually developed based on isotropic assumption. The conclusion has been further confirmed by simulations with different particle stiffness. Finally, the assumptions in the newly developed model for 2D simulation by Li and Zhang (T. Li, Y. Zhang, A new model for two-dimensional numerical simulation of pseudo-2D gas–solids

fluidized beds, Chem. Eng. Sci. 2013, 102:246–256) are examined against the DEM simulation.

Keyword: gas-solid flow, fluidized bed, computational fluid dynamics, discrete element method, particle-wall interaction, two-dimensional flow

* Corresponding author at: National Energy Technology Laboratory,

Morgantown, WV 26505, USA. Tel.: 1 304 285 4538.

E-mail addresses: tingwen.li@contr.netl.doe.gov, litingwen@gmail.com (T. Li).

1. Introduction

Pseudo-two dimensional (2D) fluidized beds, which are planar rectangular columns of limited thickness, are widely used in the experimental studies to better understand the complex flow dynamics in gas-solid systems. Benefit to the small thickness and typically transparent walls, they allow direct observation of the complex solids flow behavior such as bubble and clusters in gas-solid system through non-intrusive imaging techniques such as Particle Image Velocimetry (PIV) and Digital Image Analysis (DIA). Extensive fundamental research in pseudo-2D fluidized beds can be found in the literature on bubble properties, jet penetration, particle clustering, solids flow patterns, and solids mixing and segregation which have been utilized to improve the understanding of flow behavior in three-dimensional (3D) fluidized beds (Rowe et al. 1965; Lim et al. 1990; Caidedo et al. 2003; Busciglio et al. 2008; Goldschmidt et al. 2003; Zhong and Zhang 2005; Pallares and Johnsson 2006; Muller et al. 2007; Laverman et al. 2008; Xu and Zhu 2011; Hernandez-Jimenez et al. 2011, 2013, 2014; Sanchez-Delgado et al. 2013). The abundant qualitative and quantitative experimental data available and relatively simple geometry make the pseudo-2D system good candidate for model development and validation.

With the continuously evolvement in the computational hardware and numerical algorithms, computational fluid dynamics (CFD) has become an important tool to help understand the complex flow behavior in gas-solids fluidized beds. There are several CFD modeling approaches for gas–solid flow simulations as reviewed by van der Hoef et al. (2006). Among them, the Eulerian–Eulerian (EE) method (also called the two-fluid

model or TFM), and the Lagrangian–Eulerian (LE) method are the most widely used approaches to simulate gas–solid flows. The former treats both gas and solid phases as interpenetrating continuum with appropriate constitutive correlations. The latter treats the gas phase as continuum, but tracks the solid phase on the particle level by following the trajectory of each individual particle or a swarm of particles. Specifically, the discrete element method (DEM), also known as discrete particle method (DPM), is often used in which the solid phase is represented by individual particle and particle-particle and particle-wall collisions are directly resolved using a hard-sphere or soft-sphere model. Given the detailed information provided by DEM simulation, it has been widely used to conduct fundamental research of granular flow to develop and validate the constitutive sub-model for the continuum model (Chialvo and Sundaresan 2013; Louge 1994).

Both TFM and DEM have been used to study the flow hydrodynamics in pseudo-2D fluidized bed systems numerically. It is evident that the particle-wall interaction plays a significant role in affecting the flow behavior in lab-scale gas-solid fluidized beds especially for the pseudo-2D systems with limited thickness. The front and back walls restrict the solids movement in two directions and exert a strong friction to the solids flow which lead to quite different flow behaviors from a 3D cylindrical system (Rowe 1972; Geldart 1970; Cranfield and Geldart 1974; Glicksman 1985). However, in most numerical simulations, the pseudo-2D fluidized beds are modeled in two-dimension and the effect of the front and back walls are ignored. The wall effect in pseudo-2D gas-solid systems has been investigated in several numerical studies (Kawaguchi et al. 1998; Feng and Yu 2010; Li et al. 2010, 2012; Cloete et al. 2013). It has been demonstrated that the

frictional effect from the front and back walls, which is not considered in most 2D simulations, leads to the deviation for solids velocity and bubble rising velocity (Li et al. 2010, 2012; Cloete et al. 2013). To fully account for the wall effect, a 3D simulation is needed for accurate prediction of pseudo-2D gas-solid fluidized beds. The 3D simulation is still expensive for the DEM simulations especially for the system with fine particles. As far as the computational cost is concerned, the TFM is less expensive but requires accurate closure model and boundary conditions. In TFM, the governing equations for the solids phase are mostly closed by the kinetic granular theory (Gidaspow 1994). Different wall boundary conditions for the solids phase, i.e. free-slip, partial-slip and no-slip wall have been used in the literature. Among them, the partial-slip wall boundary condition is believed most realistic and a lot of effort has been reported in the literature to improve the accuracy of it (e.g. Johnson and Jackson 1987; Jenkins 1992; Li and Benyahia 2012; Schneiderbauer et al. 2012; Zhao et al. 2014; Soleimani et al. 2015). In the development of such wall boundary conditions, several assumptions have been used such as steady flow state at the wall and isotropic particle velocity distribution. As an accurate wall boundary condition is critical for the quantitative validation of pseudo-2D system considering the strong wall effect, detailed information on the particle-wall interaction in such system is of great value for improving the available boundary conditions. Alternatively, Li and Zhang (2013) developed a model for 2D simulations to account for the effect of front and back walls in a pseudo-2D gas-solid fluidized bed without the need of a 3D simulation. The model was developed based on the partial-slip wall boundary condition after introducing several assumptions. The results were clearly improved comparing to those obtained when the system was modelled just as a 2D plane, and the

computational cost was greatly reduced compared to the 3D simulation. However, the validity of the new model relies on the appropriateness of the wall boundary condition and assumptions used to develop the model.

In the current study, DEM simulations of a pseudo-2D gas-solid fluidized bed are reported to investigate the particle-wall interaction. Taking advantage of the detailed particle-particle and particle-wall collisions resolved by the DEM simulations, the macroscopic flow field variables used in the TFM, including solids pressure, granular temperature, normal and tangential stresses, are derived and examined. Specifically, the relationships between these field variables are analyzed which can be used to improve the wall boundary condition for the solids phase in TFM simulations. Finally, the assumptions used in the 2D flow model proposed by Li and Zhang for pseudo-2D fluidized bed simulations are examined and the validity of that model is confirmed.

2. Numerical simulations

2.1. Numerical model

The open-source MFIX-DEM code, developed at US Department of Energy's National Energy Technology Laboratory (NETL) is used to conduct the numerical simulations of a 2D bubbling fluidized bed (Garg et al. 2010). In MFIX-DEM, DEM for the solid particles is coupled with the CFD flow solver to simulate the gas-solid flow. In DEM, the position, linear and angular velocities of each particle are tracked according to Newton's laws. The inter-particle collisions are directly resolved using the soft-sphere model (based on a linear spring-dashpot model) of Cundall and Strack (1979) which treats the collision as a continuous process taking place over a finite time. The contact force is then calculated as a function of the distance between colliding particles based on physically realistic

interaction laws using empirical spring stiffness, dissipation constant, and friction coefficient. The particle–wall interaction is treated in the same way as the particle–particle collision. The gas flow is simulated by solving the averaged Navier-Stokes equations for mass and momentum conservation which account for solid volume fraction and additional coupling terms due to interactions between the two phases (Tsuji et al. 1993). The governing equations and key closure models solved in the MFIX-DEM are summarized in Table 1. Details of the governing equations along with the numerical implementation, including the coupling procedure, can be found in Garg et al. (2012) and Garg et al. (2012). The MFIX-DEM code has been verified and validated for a wide range of applications (Garg et al. 2012; Li et al. 2013).

Table 1.

2.2. Simulated Setup

A pseudo-2D cold flow fluidized bed of dimensions 0.3 m × 1 m × 0.01 m as schematically shown in Fig. 1 is considered in the current study. Detailed information on the experimental setup and test can be found in (Hernández-Jiménez et al. 2013). The front and rear walls of the bed were made of glass for visual observation. Air at room temperature was fed through a perforated distributor to fluidize the bed material. The distributor consisted of two rows of 30 holes of diameter 1 mm arranged in a triangular configuration with 1 cm pitch. Experimental tests using the ballotini glass beads with density of 2500 kg/m^3 and size range of 0.6-0.8 mm were simulated. Without detailed measurement of the particle size distribution, the intermediate particle diameter of 0.7 mm was used in the simulation.

Fig. 1.

A static bed height of 0.3 m which results in about 3 million particles inside the system was simulated. The bed is fluidized by air at a superficial gas velocity of 0.88 m/s which corresponds to two times the minimum fluidization velocity of 0.44 m/s measured experimentally (Hernández-Jiménez et al. 2013). The numerical parameters used in the simulations are listed in Table 2. These parameters maintain constant for all simulations unless noted for the parametric study. A parametric study for the coefficient of friction for inter-particle and particle-wall collisions was carried out as it is believed to be the most critical parameter in the frictional forces of the walls acting on the particles. In addition, a parametric study for the particle spring constant was conducted to investigate its influence on the simulation results. In the DEM simulation, rotation of each particle is tracked explicitly and its contribution to the particle-wall interaction is accounted in the analysis. However, the effect of rolling friction is not considered in the current study as the numerical study of a similar system suggested that the particle rotational kinetic energy is negligible comparing to the translational kinetic energy (Li et al. 2012).

Table 2.

A uniform grid size of 5 mm (7 times the particle size) is used for the CFD solver to discretize the 3D computational domain which leads to two cells in the thickness direction. The wall effect is mainly accounted for by the solids flow through particle-wall interactions. Ideally, the gas velocity at the wall is zero and a no-slip wall boundary condition should be used. It should be noted that there exists strong gradient in the gas flow along the thickness direction mainly caused by the particle flow in the other two directions. A boundary layer with a thickness of the order of one particle diameter is expected. However, the detailed gas flow behavior near the wall within 1- or 2-particle layer is beyond the current model capability of CFD-DEM solving averaged Navier-Stokes equations with numerical grid greater than particle size (Li et al. 2012). In this study, the variation of gas flow in the thickness direction is implicitly ignored and a free-slip wall boundary condition is used for the gas phase at the front and rear walls. In addition, one case with 2.5 mm grid size in the thickness direction is conducted to confirm that the results are not sensitive to the grid size in that direction. Gas flow is fed through dispersed cells in the bottom boundary to mimic the perforated distributor used in the experiment. Limited by the grid resolution, 20 holes in the distributor were simulated to promote the bubble formation introduced by the jet collapsing observed in the experiment. The gas flow then leaves the computational domain through the top boundary at a constant pressure. A no-slip boundary condition is used for the gas phase at the left and right side walls for simplicity. The effect of gas phase wall boundary condition might become important for certain applications (Beetstra et al. 2007). No further investigation on the effect of left and right wall boundary conditions for the gas

phase is conducted as the current study mainly focuses on the particle-wall interaction from the front and back walls.

All simulations were run in the hybrid parallel mode by coupling Distributed Memory Parallel (DMP) and Shared Memory Parallel (SMP) using Message Passing Interface (MPI) and OpenMP on NETL's supercomputer, HPCEE (Liu et al. 2014; Gopalakrishnan and Tafti 2013). Transient simulation results were saved at a frequency of 100Hz and each simulation reached 10 seconds of physical time for analysis.

3. Results and discussion

3.1. Comparison to experimental observation

Fig. 2 shows two snapshots taken from the experimental test and numerical simulation for qualitative comparison. In both figures, the light color corresponds to high solids concentration and dark color corresponds to bubble or freeboard with low solids concentration. The small gas jets formed above the distributor orifices can be observed from the experimental image which is reasonably captured by the numerical simulation. Small bubbles formed near the distributor grow and collapse as they rise. Large bubbles finally burst at the bed surface. The numerical result shows smoother bubble surface than the experimental image mainly in the spherical capped region. The slight difference might be attributed to the particle size distribution in the bed material. Overall, the numerical simulation predicts reasonably agreeable bubbling behavior as observed in the experiment.

Fig. 2.

In addition to the qualitative comparison to the experimental observation, the DEM simulation results have been used to characterize the overall wall frictional force (Hernández-Jiménez et al. 2014). Based on the force balance model proposed by Hernández-Jiménez et al. (2013), the overall frictional force due to particle-wall interaction was estimated and found consistent with the experimental analysis. In addition, the DEM results corroborated that the overall frictional force can be considered equal to the velocity of the center of mass times a particle–wall interaction coefficient, c. Furthermore, a local estimation of the coefficient c was performed by analyzing the vertical component of the tangential force of the particle–wall collisions and the vertical particle velocity. It was found that the most probable value of the local coefficient c in the DEM simulations is similar to the global value experimentally obtained. Given the qualitative and quantitative consistency to the experiment, the DEM simulation results reported in Hernández-Jiménez et al. (2014) are further analyzed to investigate the detailed particle-wall interaction in the pseudo-2D column. Specifically, the current study seeks a more fundamental approach to characterize the particle-wall interaction which can be leveraged to improve the boundary conditions used in the TFM simulations of pseudo-2D systems.

3.2. Characterization of particle-wall interaction

To better understand the particle-wall interaction, the macroscopic flow variables typically used in the TFM, such as solids stress tensor, granular temperature, are extracted. To derive the continuous field variables from the DEM simulation results, appropriate spatial window size is needed for the data analysis. For the CFD-DEM simulation, it is natural to choose the fluid cell as the window for calculating the macroscopic field variables. By summing up the particle-wall contact force, $\mathbf{F}_{iW}$, for each particle in contact with the wall, the stress exerted by the particles on the wall can be calculated as

$$\mathbf{T}_W = \frac{1}{A}\sum_{i \in W} \mathbf{F}_{iw} \tag{1}$$

where A is the surface area of the wall cell.

The normal and tangential components of the wall stress are

$$T_n = \mathbf{n} \cdot \mathbf{T}_W \tag{2}$$

and

$$T_s = \left| \mathbf{T}_W - \mathbf{n} T_n \right| \tag{3}$$

where $\mathbf{n}$ is the unit vector normal to the wall.

The granular temperature, Θ, is calculated as

$$\Theta = \frac{1}{3N}\sum_{i=1}^{N} (\mathbf{u}_i - \bar{\mathbf{u}}) \cdot (\mathbf{u}_i - \bar{\mathbf{u}}) \tag{4}$$

where N is the number of particle in the computational cell, m_i is the mass of particle, $\mathbf{u}_i$ is the particle velocity vector, and $\bar{\mathbf{u}}$ is the instantaneous spatially-averaged solids velocity in the cell which is calculated as

$$\bar{\mathbf{u}} = \frac{1}{N}\sum_{i=1}^{N}\mathbf{u}_i \tag{5}$$

The macroscopic solid stress tensor, $\boldsymbol{\sigma}$, is calculated in each computational cell as (Chialvo et al. 2012)

$$\boldsymbol{\sigma} = \frac{1}{V}\sum_{i=1}^{N}\left[\sum_{j\neq i}\frac{1}{2}\mathbf{r}_{ij}\mathbf{F}_{ij} + m_i\left(\mathbf{u}_i - \bar{\mathbf{u}}\right)\left(\mathbf{u}_i - \bar{\mathbf{u}}\right)\right] \tag{6}$$

where $\mathbf{r}_{ij}$ is the vector from center of particle j to center of particle i and $\mathbf{F}_{ij}$ is the contact force between the colliding particles, and V is the volume of the domain for analysis, i.e. the computational cell. The solids pressure defined as the average of the diagonal terms of the solids stress tensor, i.e. $P_s = 1/3\left(\sigma_{11} + \sigma_{22} + \sigma_{33}\right)$ can be calculated as

$$P_s = \frac{1}{3V}\sum_{i=1}^{N}\left[\sum_{j\neq i}\frac{1}{2}\mathbf{r}_{ij}\cdot\mathbf{F}_{ij}\right] + \rho_p\varepsilon_s\Theta \tag{7}$$

The first term of Eq. (6) originates from the particle-particle interactions in form of instantaneous collision or long-time frictional contact. The second term stands for the kinetic contribution to the solids pressure (Gidaspow 1994). It should be noted that the calculated quantities might be affected by the number of particles inside the sampling window. For example, granular temperature and solids pressure might demonstrate substantial statistical error for cells inside a bubble or in the freeboard region due to the limited number of particles there. In the current study, we mainly focus on the dense emulsion phase for which the number of particles in a computational cell is believed to be sufficient for the calculation (Gopalan and Shaffer 2013).

Fig. 3 shows the transient snapshots of the calculated field variables. Fig. 3(a) presents the solids concentration distribution inside the bed. The solids pressure calculated based

on Eq. (6) is shown in Fig. 3(b) and the kinetic contribution i.e. the second term in the right-hand side of Eq. (6), is shown in Fig. 3(c). As can be seen from these figures, the solids pressure is high in the dense emulsion phase and low in the dilute bubble region. Due to higher solids velocities and stronger solids interactions, the solids pressure in the bubble wake is especially higher than other areas. The kinetic component of solids pressure is mainly in the lower bubble wake area where the granular temperature as shown in Fig. 3(f) is high. As revealed by the simulations, the kinetic part of solids pressure shown in Fig. 3(c) is negligible comparing to the first part in equation (6). In the following analysis, the kinetic part of the solids pressure is ignored and only the component from inter-particle contacts is used. The normal and tangential components of the stress on the wall exerted by the particles are shown in Fig. 3(d) and 2(e). From the transient snapshots, it can be seen that there tends to be a strong correlation between the solids pressure and the stress on the wall.

Fig. 3.

In the following analysis, mainly the particle-wall interaction for the emulsion phase is investigated. For this purpose, the solids pressure and wall stresses in each computational cell are extracted for the emulsion phase. To distinguish the emulsion phase and the bubble phase, a voidage of 0.7 is used. Different values for voidage have been used in the literature to demarcate bubble boundaries. Here a low value of 0.7 is used so that the analyses are focusing on the dense emulsion phase which has less statistical error. A large amount of data has been extracted from the transient simulation results covering hundreds

of frames for analysis. Fig. 4 plots the values of normal wall stress versus the solids pressure for each computational cell collected over a 4 s simulation period. About half million points are plotted in the figure. As can be seen, the normal wall stress demonstrates clear dependence on the solids pressure. The calculated normal wall stress increases with the solids pressure. According to the definition, the normal wall stress equals to σ_{33} at the wall which is the solids stress component in the normal wall direction. Hence, the difference between normal wall stress and the solids pressure shown here indicates the strong anisotropy in the flow. A simple linear regression can be used to derive the relationship between these two variables as shown in the figure. The reported R-Square of 0.8161 indicates the linear fitting reasonably captures the correlation between normal wall stress and the solids pressure. In particular, the normal wall stress is of the order of 7% of the solids pressure. The anisotropic flow behavior is believed to be related to gravitation, dominant flow direction, and wall effect. Clearly, the particle movement in the thickness direction is limited because of the wall effect and is less vigorous comparing to the other two directions. Hence the normal force on the wall exerted by the particle flow is much lower comparing to the solids pressure which is the average of three orthogonal normal stresses.

To better quantify the relationship between the normal wall stress and solids pressure, the large amount of data shown in Fig. 4 has been binned in small intervals with respect to the solids pressure then average and standard deviation of the normal wall stress are calculated as shown in Fig. 5. In Fig. 5, the symbols are the average normal wall stress and the error bars represent ± one standard deviation for data in each bin. A linear

correlation can be obtained by fitting the average data which yields the similar relationship as the linear regression of the raw data in Fig. 4. The equation has been shown in the figure where x corresponds to the x-axis variable, i.e. the solids pressure and y corresponds to the y-axis variable, i.e. the normal wall stress. It should be noted that the results for high solids pressure are not included in Fig. 5 as there are not sufficient data points for averaging (a cut-off criterion of 100 is used here).

Fig. 4.

Fig. 5.

To further investigate the anisotropic flow behavior encountered in the current pseudo-2D system. The granular temperature is decomposed into three components

$$\Theta = \Theta_x + \Theta_y + \Theta_z \tag{7}$$

where Θ_x, Θ_y, and Θ_z account for the contribution from different velocity components. As shown in Fig. 6, the magnitudes of different components of granular temperature are different. Most of granular temperature originates from the fluctuating velocity in the vertical direction which is the dominant flow direction. The presence of front and back walls confines the particle movement as well as its fluctuation in the thickness direction. Hence, the granular temperature contributed by the fluctuating solids velocity in the thickness direction is much less than those from the vertical and horizontal directions. This is consistent with the anisotropic behavior observed above for the solids stress tensor. The strong anisotropic flow behavior in pseudo-2D systems should be awared in

TFM simulation for which the constitutive correlation and boundary condition for the solids phase are developed based on the isotropic flow assumption.

Fig. 6.

Similar analysis is conducted for the tangential and normal wall stresses as shown in Fig. 7. Again, the linear relationship has been obtained which is consistent with the standard friction equation. Hence, the slope of the fitted line can be interpreted as an effective coefficient of friction between the particles flow and wall.

$$T_s = \mu_{eff} T_n \tag{8}$$

The predicted effective friction coefficient of 0.2555 is lower than that of 0.6 for the particle and wall surface. The standard friction equation using the physical particle-wall friction coefficient has been shown as a dashed line in Fig. 7 for comparison. According to the rigid-body theory, only two possible rebound behaviors corresponding to sliding and non-sliding collision exist for a rigid spherical body colliding with the wall (Li and Benyahia 2012). For a sliding particle-wall collision, the normal and tangential forces can be described by the Coulomb law. For a non-sliding collision, the relative displacement of the contact point does not occur so that the sphere is rolling on the surface during the contact which results in much lower friction comparing to the sliding collision. Hence the overall effective friction coefficient is lower than the coefficient of friction specified for the sliding particle-wall contact. The interaction between the particle flow and wall would be more complicated than depicted by the rigid body theory. The current DEM

implementation is capable of capturing the aforementioned contacts which makes it an ideal tool for investigating the particle-wall interactions.

Fig. 7.

It should be noted that the effective friction coefficient derived from fitting the transient data fluctuates slightly. To obtain the representative relationship between normal and tangential forces, sufficient sample points are needed to reduce the statistical error. In the whole study, data collected in 2s with a data saving frequency of 100Hz are used after careful examination of the effective frictional coefficients obtained from different sample periods ranging from 0.1 to 8s.

3.3. Effective frictional coefficient

A parametric study of the friction coefficient has been conducted by varying it from 0.3 to 0.7. In the current study, the same friction coefficients are used for both particle-particle and particle-wall interactions since the bed material and wall material can be considered similar. Fig. 8 plots the normal wall stress versus the solids pressure for the emulsion phase for simulations with different friction coefficients. For different conditions, the linear relationship fits the data reasonably well. The slopes of the linear fitting are close and no general trend can be obtained. The results tend to indicate the friction coefficient has no significant influence on the anisotropy in stress tensor.

Fig. 8.

Fig. 9 shows the tangential wall stress versus the normal wall stress for different friction coefficients. It should be noted that the data points become more scattered as the friction coefficient increases which can be seen from the increasing standard deviations in the figure. Overall, the linear relationship still reasonably describes the data though the fitting becomes less accuracy for high friction coefficients. The slope of a linear fitting, i.e. the effective friction coefficient, increases as the particle-particle and particle-wall friction coefficient increases for friction coefficients of 0.3, 0.4 and 0.5. It slightly decreases for friction coefficients of 0.6 and 0.7 which is mainly attributed to the less accurate fitting for both cases. The linear regression of the raw data points is also used to evaluate the dependence of effective frictional coefficient on the physical particle-wall friction coefficient. Overall, the effective friction coefficient increases slightly as the particle-particle and particle-wall friction coefficient increases from 0.3 to 0.7. However, the low increase in the effective friction coefficient comparing to the change in physical friction coefficient suggests only a moderate dependence on the friction coefficient.

Fig. 9.

3.4. Effect of spring constant

In the linear spring-dashpot soft-sphere model used in the current study, the time for particle collision is expressed as a function of particle size and hardness. To avoid extremely small time step for the simulation, a lower spring constant is typically used in the CFD-DEM simulations which usually does not affect the simulation results (Tsuji et al. 1993). It has been a typical exercise to speedup DEM simulation by reducing the particle stiffness to make particles less stiff or softer to allow a larger time step (Malone and Xu 2008). On the other hand, some studies have suggested that reduction in particle stiffness can lead to undesirable effects. For example, properties such as the bulk stiffness and bulk restitution of granular flow changed as a result of the stiffness reduction (Lommen et al. 2014). The spring constant in the contact force model affects the rebound and sticking behavior of the collision of cohesive fine particles in gas-solid fluidized bed (Kobayashi et al. 2013). Hence, it is important to verify the simulation results are not affected by the particle stiffness substantially.

To investigate the effect of particle stiffness, two simulations with the normal spring constant of 20000 and 200000 N/m for particle-particle and particle-wall interactions were conducted for the friction coefficient of 0.6. It should be noted that as the spring constant increases, the duration of collision between two particles decreases proportionally to the square root of the spring constant. Hence the time step required for accurate resolution of particle contact has to be reduced which results in much longer CPU time. To alleviate the extreme computational cost associated with high spring constants, only 2 s simulations were completed by restarting from the run with the spring constant of 2000 N/m. The results of the last second are analyzed.

During the data analysis, it was found that the calculated field variables, i.e. solids pressure and wall stresses for the runs with high spring constants are highly dispersed comparing to the results shown above. After careful examination, it is determined that the default window of one fluid cell for analysis is not sufficient to derive the macroscopic field variable without significant statistical noise. This is mainly because of the less particle contacts captured by the instantaneous snapshot of the simulation due to the reduced duration of collision. On the other hand, the increased contact force between two colliding particles further introduces more statistical noises. To overcome this, the sampling window has been extended from 1 fluid cell to 2×2, 3×3 and 4×4 fluid cells. As shown in Fig. 10, there exist more and more evident correlation between normal wall stress and the solids pressure as the sampling window is extended. To confirm this, averaged data and its standard deviation after binning with respect to the solids pressure are shown in Fig. 11 for different window sizes. Clearly, increasing the sampling widow reduces the standard deviation and leads to better fitting to the averaged data. The following results are based on the sampling window of 3×3 fluid cells.

Fig. 10.

Fig. 11.

Fig. 12 shows the relationship between solids pressure and normal wall stress as predicted by different spring constants using the 3×3 fluid cells for analysis. Comparing

to the results shown in Fig. 5, the increased window size reduce the standard deviation of the data for the case with low spring constant of 2000 N/m in Fig. 12(a). However, the effective friction coefficients through data fitting are comparable which suggests the sampling window size of 1 cell is appropriate for simulations with low spring constant. In Fig. 12, the data become less correlated between solids pressure and normal wall stress for simulation with higher spring constants as indicated by the increasing stand deviations. This is believed to be related to the statistical noise due to high particle stiffness. Overall, the linear relationship fits all data reasonably well and the slopes remain almost constant for different values of particle stiffness.

Fig. 12.

Fig. 13 shows the tangential wall stress versus the normal wall stress for simulations with different spring constants. Similarly, the data become less correlated for higher spring constants due to the increased statistical noise. The linear relationship can be easily observed in the average data. The slope of a linear fitting, i.e. the effective friction coefficient, increases slightly as the particle spring constant is increased which suggests the particle stiffness does affect the particle-wall interaction to some extent. Considering the small difference in the fitting slope, the effect is deemed negligible. However, attention on the particle stiffness is needed for the DEM study when accurate quantitative prediction on particle-particle and particle-wall contact forces is sought.

Fig. 13.

3.5 Effect of grid resolution in thickness direction

To investigate the effect of grid resolution in the thickness direction, one simulation with refined grid in that direction was conducted for the friction coefficient of 0.6. For this case, the grid sizes in the other two directions were maintained the same. No other change was made except the numerical grid. The mean flow hydrodynamics with respect to solid distribution and movement were compared against the results of 5 mm grid which showed good consistency. Given the good 2D flow behavior of the pseudo-2D system, the results confirm that the grid resolution in the thickness direction has no significant effect on results. It should be noted that there exist several issues related to the DEM simulation when the dimension of computational cell is too small comparing to the particle size due to the large grid size required by the CFD–DEM coupling. Hence no further grid refinement study was conducted. Similar analyses were carried out to extract the field variables. Fig. 14(a) shows the relationship between solids pressure and normal wall stress predicted by the simulation with 2.5 mm grid in the thickness direction. The ratio between normal wall stress and solids pressure is about 0.04 which is smaller than that of 0.0756 shown in Fig. 5. This tends to suggest that stronger anisotropy exists in the particle force network as approaching the wall. Fig. 14(b) plots the tangential wall stress versus the normal wall stress. The fitted effective friction coefficient of 0.2471 is close to that of 0.2555 shown in Fig. 7 which indicates the grid resolution in the thickness direction has only negligible effect on the particle-wall interaction for the current pseudo-2D system.

Fig. 14.

3.6. Revisiting Li and Zhang's model

Li and Zhang (2013) developed a 2D model for TFM simulations to account for the front and back wall effects in a pseudo-2D gas-solid fluidized bed. In this model, the collisions between particles and the front and back walls are assumed to be sliding. The shear stress S exerted by the wall is then calculated as

$$S = \mu N \tag{8}$$

where N is the normal wall stress. The normal wall stress is estimated from the solids pressure calculated in the 2D simulation. With the 2D flow assumption, the shear force imposed by the front and back walls can be interpreted as a body force acting on the solids flow.

The DEM simulation results here can be used to verify the assumptions used in Li and Zhang's model. Clearly, the normal wall stress is much lower than the solids pressure due to the strong anisotropic flow behavior. The anisotropy in solids stress should be considered when the solids pressure is used to approximate the normal wall stress. Furthermore, an effective friction coefficient should be used in equation (8) instead of the particle-wall friction coefficient. As demonstrated above, the effective friction coefficient is much lower than the particle-wall frication coefficient. On the other hand, there exists a linear relationship between the shear stress and the solids pressure which make it possible

to account for the wall effect in a 2D simulation through a single parameter lumping the flow anisotropy and the effective friction coefficient together. However, one might need certain calibration steps to determine its appropriate value based on the experimental data.

4. Conclusion

For the pseudo-2D gas-solid system investigated, there exists a strong correlation between the normal stress and tangential stress at the wall in the dense emulsion phase. An effective frictional coefficient can be used to reasonably describe the relationship. The effective frictional coefficient is lower than the particle-wall frictional coefficient. It slightly increases with the particle-wall frictional coefficient. There exist significant anisotropic behaviors in solids stress and granular temperature. The normal wall stress is much lower than the solids pressure and the granular temperature component in the thickness direction is lower than those in the other two directions. The strong anisotropic behaviors in the pseudo-2D system pose challenge to TFM simulation for which the constitutive correlation and boundary condition for the solids phase are mainly developed based on the isotropic assumption. In addition, the assumptions in the 2D model for a pseudo-2D gas-solid system by Li and Zhang (2013) are examined and the flow anisotropy and the effective friction coefficient are suggested to be considered in the model. The simple 2D model is considered a reasonable simplification by lumping the flow anisotropy and the effective friction coefficient together through a single parameter.

In the current CFD-DEM study, the spring constant, which characterizes the particle stiffness, affects the force analysis to certain extent although it does not alter the qualitative conclusion. Special attention is needed for data analysis when using DEM to investigate the particle-particle and particle-wall interaction especially when the quantitative prediction is sought. Overall, CFD-DEM has been demonstrated a very useful tool for detailed investigation of gas-solids flow.

Nomenclature

$\boldsymbol{\sigma}$	stress	Pa
ε	volume fraction	-
μ	friction coefficient	-
μ_g	gas viscosity	Pa.s
$\boldsymbol{\omega}$	angular velocity	rad/s
ρ	density	kg/m^3
Θ	granular temperature	m^2/s^2
A	area	m^2
d	diameter	m
F	force	N
$\mathbf{g}$	gravity	m/s^2

I	momentum of inertia	$kg.m^2$
m	mass	kg
N	normal wall stress	Pa
P	pressure	Pa
S	tangential wall stress	Pa
t	time	s
T	stress	Pa
$\mathbf{T}$	torque	J
$\mathbf{u}$	particle velocity	m/s
$\mathbf{v}$	gas velocity	m/s
U	velocity	m/s
V	volume	m^3
$\mathbf{x}$	position	m

Acknowledgments

This technical report was produced in support of the National Energy Technology Laboratory's ongoing research in advanced numerical simulation of multiphase flow under the RES contract DE-FE0004000.

Disclaimer

This report was prepared as an account of work sponsored by an agency of the United States Government. Neither the United States Government nor any agency thereof, nor any of their employees, makes any warranty, express or implied, or assumes any legal liability or responsibility for the accuracy, completeness, or usefulness of any information, apparatus, product, or process disclosed, or represents that its use would not infringe privately owned rights. Reference herein to any specific commercial product, process, or service by trade name, trademark, manufacturer, or otherwise does not necessarily constitute or imply its endorsement, recommendation, or favoring by the United States Government or any agency thereof. The views and opinions of authors expressed herein do not necessarily state or reflect those of the United States Government or any agency thereof.

References:

Beetstra R, van der Hoef MA, Kuipers JAM. Numerical study of segregation using a new drag force correlation for polydisperse systems derived from lattice-Boltzmann simulations. Chem. Eng. Sci. 2007; 62, 246–255.

Busciglio A, Vella G, Micale G, Rizzuti L. Analysis of the bubbling behaviour of 2D gas solid fluidized beds, Chem. Eng. J. 2008; 140:398–413.

Caicedo GR, Marqués JJP, Ruíz MG, Soler JG. A study on the behaviour of bubbles of a 2D gas–solid fluidized bed using digital image analysis, Chem. Eng. Process. Process Intensif. 2003; 42:9–14.

Chialvo S, Sundaresan S. A modified kinetic theory for frictional granular flows in dense and dilute regimes, Phys. Fluids. 2013; 25:070603.

Chialvo S, Sun J, Sundaresan S. Bridging the rheology of granular flows in three regimes, Phys. Rev. E. 2012; 85:021305.

Cloete S, Zaabout A, Johansen ST, van Sint Annaland M, Gallucci F, Amini S. The generality of the standard 2D TFM approach in predicting bubbling fluidized bed hydrodynamics, Powder Technol. 2013; 235:735–746.

Cranfield RR, Geldart D. Large particle fluidisation, Chem. Eng. Sci. 1974; 29:935–947.

Cundall PA, Strack ODL. A discrete numerical model for granular assemblies, Géotechnique. 1979; 29:47–65.

Feng YQ, Yu AB, Effect of bed thickness on the segregation behavior of particle mixtures in a gas fluidized bed, Ind. Eng. Chem. Res. 2010; 49: 3459–3468.

Garg R, Galvin J, Li T, Pannala S. Documentation of open-source MFIX-DEM software for gas-solids flows. 2012; https://mfix.netl.doe.gov/download/mfix/mfix_current_documentation/dem_doc_2012-1.pdf.

Garg R, Galvin J, Li T, Pannala S. Open-source MFIX-DEM software for gas–solids flows: Part I—Verification studies, Powder Technol. 2012; 220:122–137.

Geldart D. The size and frequency of bubbles in two- and three-dimensional gas-fluidised beds, Powder Technol. 1970; 4:41–55.

Gidaspow D. Multiphase flow and fluidization: continuum and kinetic theory descriptions, Academic Press, 1994.

Glicksman LR, McAndrews G. The effect of bed width on the hydrodynamics of large particle fluidized beds, Powder Technol. 1985; 42:159–167.

Goldschmidt MJV, Link JM, Mellema S, Kuipers JAM. Digital image analysis measurements of bed expansion and segregation dynamics in dense gas-fluidised beds, Powder Technol. 2003; 138:135–159.

Gopalakrishnan P, Tafti D. Development of parallel DEM for the open source code MFIX, Powder Technol. 2013; 235:33–41.

Gopalan B, Shaffer F. Higher order statistical analysis of Eulerian particle velocity data in CFB risers as measured with high speed particle imaging, Powder Technol. 2013; 242:13–26.

Hernández-Jiménez F, Li T, Cano-Pleite E, Rogers W, Acosta-Iborra A. Characterization of the particle–wall frictional forces in pseudo-2D fluidized beds using DEM, Chem. Eng. Sci. 2014; 116:136–143.

Hernández-Jiménez F, Sánchez-Delgado S, Gómez-García A, Acosta-Iborra A. Comparison between two-fluid model simulations and particle image analysis & velocimetry (PIV) results for a two-dimensional gas–solid fluidized bed, Chem. Eng. Sci. 2011; 66:3753–3772.

Hernández-Jiménez F, Sánchez-Prieto J, Soria-Verdugo A, Acosta-Iborra A. Experimental quantification of the particle–wall frictional forces in pseudo-2D gas fluidised beds, Chem. Eng. Sci. 2013; 102:257–267.

Jenkins JT. Boundary conditions for rapid granular flows: flat, frictional walls. J Appl Mech. 1992; 59:120–127.

Johnson PC, Jackson R. Frictional collisional constitutive relations for antigranulocytes-materials, with application to plane shearing. J Fluid Mech. 1987;176:67–93.

Kawaguchi T, Tanaka T, Tsuji Y. Numerical simulation of two-dimensional fluidized beds using the discrete element method (comparison between the two- and three-dimensional models), Powder Technol. 1998; 96:129–138.

Kobayashi T, Tanaka T, Shimada N, Kawaguchi T. DEM–CFD analysis of fluidization behavior of Geldart Group A particles using a dynamic adhesion force model, Powder Technol. 2013; 248:143–152.

Laverman JA, Roghair I, van S. Annaland M, Kuipers JAM. Investigation into the hydrodynamics of gas–solid fluidized beds using particle image velocimetry coupled with digital image analysis, Can. J. Chem. Eng. 2008; 86:523–535.

Li T, Benyahia S. Revisiting Johnson and Jackson boundary conditions for granular flows. AIChE J. 2012; 58:2058–2068.

Li T, Grace J, Bi X. Study of wall boundary condition in numerical simulations of bubbling fluidized beds, Powder Technol. 2010; 203:447–457.

Li T, Gopalakrishnan P, Garg R, Shahnam M. CFD–DEM study of effect of bed thickness for bubbling fluidized beds, Particuology. 2012; 10:532–541.

Li T, Zhang Y. A new model for two-dimensional numerical simulation of pseudo-2D gas–solids fluidized beds, Chem. Eng. Sci. 2013; 102:246–256.

Li T, Garg R, Galvin J, Pannala S. Open-source MFIX-DEM software for gas-solids flows: Part II — Validation studies, Powder Technol. 2012; 220:138–150.

Li T, Benyahia S. Revisiting Johnson and Jackson boundary conditions for granular flows, AIChE J. 2012; 58:2058–2068.

Liu H, Tafti DK, Li T. Hybrid parallelism in MFIX CFD-DEM using OpenMP, Powder Technol. 2014; 259:22–29.

Lim KS, Agarwal PK, O'neill BK. Measurement and modelling of bubble parameters in a two-dimensional gas-fluidized bed using image analysis, Powder Technol. 1990; 60:159–171.

Louge MY. Computer simulations of rapid granular flows of spheres interacting with a flat, frictional boundary, Phys. Fluids. 1994; 6: 2253.

Lommen S, Schott D, Lodewijks G. DEM speedup: Stiffness effects on behavior of bulk material, Particuology. 2014; 12:107–112.

Malone KF, Xu BH. Determination of contact parameters for discrete element method simulations of granular systems, Particuology. 2008; 6:521–528.

Müller CR, Davidson JF, Dennis JS, Hayhurst AN. A study of the motion and eruption of a bubble at the surface of a two-dimensional fluidized bed using Particle Image Velocimetry (PIV), Ind. Eng. Chem. Res. 2007; 46:1642–1652.

Pallarès D, Johnsson F. A novel technique for particle tracking in cold 2-dimensional fluidized beds—simulating fuel dispersion, Chem. Eng. Sci. 2006; 61:2710–2720.

Rowe PN, Partridge BA, Cheney AG, Henwood GA. The mechanisms of solids mixing in fluidized beds, Trans. Institutetution Chem. Eng. 1965; 43:271–286.Rowe PN. Fluidised bed bubbles viewed by X-rays Part II- The transition from two to three dimensions of undisturbed bubbles, Chem. Eng. Res. Des. 1972; 50:49–54.

Sánchez-Delgado S, Marugán-Cruz C, Soria-Verdugo A, Santana D. Estimation and experimental validation of the circulation time in a 2D gas–solid fluidized beds, Powder Technol. 2013; 235:669–676.

Schneiderbauer S, Schellander D, Loderer A, Pirker S. Non-steady state boundary conditions for collisional granular flows at flat frictional moving walls. Chem. Eng. Sci. 2012; 43:149–156.

Soleimani A, Schneiderbauer S, Pirker S. A comparison for different wall-boundary conditions for kinetic theory based two-fluid models, Int. J. Multiphase Flow 2015; 17:94-97.Tsuji Y, Kawaguchi T, Tanaka T. Discrete particle simulation of two-dimensional fluidized bed, Powder Technol. 1993; 77:79–87.

van der Hoef MA, Ye M, van Sint Annaland M, Andrews AT, Sundaresan S, Kuipers JAM. Computational Fluid Dynamics, Elsevier, 2006.

Xu J, Zhu JX. Visualization of particle aggregation and effects of particle properties on cluster characteristics in a CFB riser, Chem. Eng. J. 2011; 168:376–389.

Zhao Y, Zhong Y, He Y, Schlaberg HI. Boundary conditions for collisional granular flows of frictional and rotational particles at flat walls. AIChE J. 2014; 60: 4065–4075.

Zhong W, Zhang M. Jet penetration depth in a two-dimensional spout–fluid bed, Chem. Eng. Sci. 2005; 60:315–327.

List of Figures

Fig. 1. Schematic of the pseudo-2D gas-solid fluidized bed under investigation. 3

Fig. 2. Snapshots of solids distribution from (a) experiment and (b) numerical simulation (Numerical simulation: U_g=0.88 m/s, μ_{fric}=0.6). 4

Fig. 3. Snapshots of different field variables (a) solids concentration, (b) solids pressure, (c) kinetic contribution to the solids pressure, (d) normal wall stress, (e) tangential wall stress, (f) granular temperature. (Numerical simulation: U_g=0.88m/s, μ_{fric}=0.6). 5

Fig. 4. Raw data of normal wall stress versus solids pressure for the emulsion phase together with a linear regression (Numerical simulation: U_g=0.88m/s, μ_{fric}=0.6). 6

Fig. 5. Averaged normal wall stress versus solids pressure for the emulsion phase (the symbols are average data and error bars representing ± one standard deviation; Numerical simulation: U_g=0.88m/s, μ_{fric}=0.6). 7

Fig. 6. Components of granular temperature in (a) x, (b) y and (c) z directions. (Numerical simulation: U_g=0.88m/s, μ_{fric}=0.6). 8

Fig. 7. Averaged tangential wall stress versus normal wall stress for the emulsion phase (the symbols are average data and error bars representing ± one standard deviation; the solid line is liner fitting; the dashed line represent equation (8) with the slope of physical particle-wall friction coefficient, Numerical simulation: U_g=0.88m/s, μ_{fric}=0.6).....9

Fig. 8. Averaged normal wall stress versus solids pressure for the emulsion phase for different friction coefficients (a) μ_{fric}=0.3; (b) μ_{fric}=0.4; (c) μ_{fric}=0.5; (d) μ_{fric}=0.7. 11

Fig. 9. Averaged tangential wall stress versus normal wall stress for the emulsion phase for different friction coefficients (a) μ_{fric}=0.3; (b) μ_{fric}=0.4; (c) μ_{fric}=0.5; (d) μ_{fric}=0.7.. 13

Fig. 10. Normal wall stress versus solids pressure in the emulsion phase for the simulation with spring constant of 200000 N/m using different window sizes (Numerical simulation: U_g=0.88m/s, μ_{fric}=0.6). 14

Fig. 11. Averaged normal wall stress versus solids pressure in the emulsion phase for the simulation with spring constant of 200000 N/m using different window sizes (a) 1×1, (b) 2×2, (c) 3×3, (d) 4×4 (Numerical simulation: U_g=0.88m/s, μ_{fric}=0.6). 16

Fig. 12. Normal wall stress versus solids pressure for the emulsion phase together with a linear regression for different spring constant (a) 2000 N/m; (b) 20000 N/m; (c) 200000 N/m (Numerical simulation: U_g=0.88m/s, μ_{fric}=0.6). 18

Fig. 13. Tangential wall stress versus normal wall stress for the emulsion phase together with a linear regression for different spring constant (a) 2000 N/m; (b) 20000 N/m; (c) 200000 N/m (Numerical simulation: U_g=0.88m/s, μ_{fric}=0.6). 20

Fig. 14. Results predicted by 2.5 mm grid in the thickness direction (a) Normal wall stress versus solids pressure; (b) Tangential wall stress versus normal wall stress (Numerical simulation: U_g=0.88m/s, μ_{fric}=0.6). 21

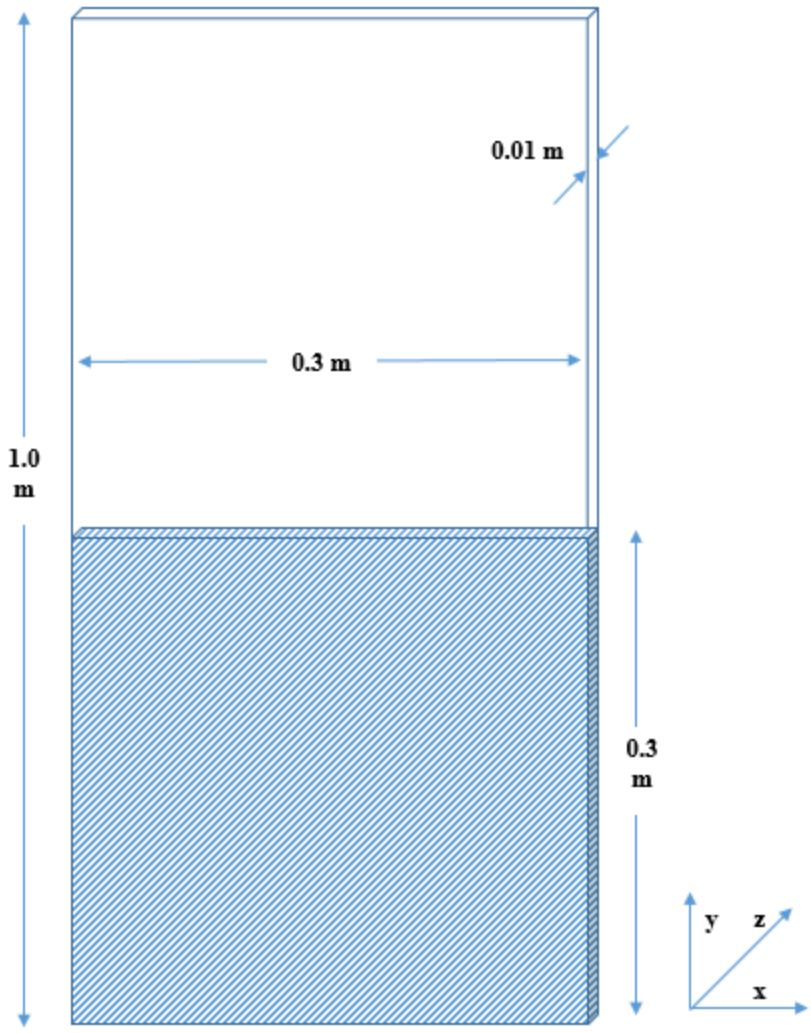

Fig. 1. Schematic of the pseudo-2D gas-solid fluidized bed under investigation.

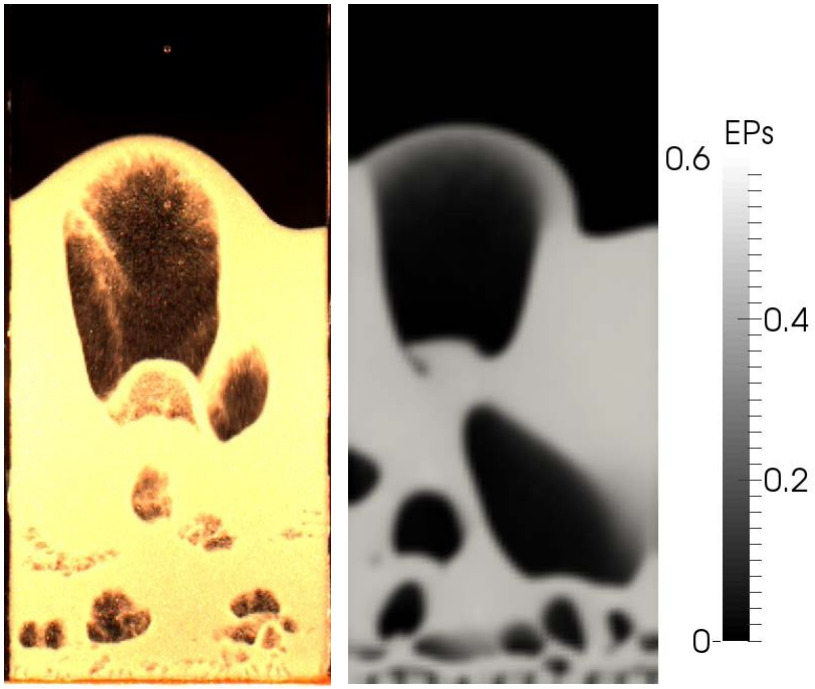

(a) (b)

Fig. 2. Snapshots of solids distribution from (a) experiment and (b) numerical simulation (Numerical simulation: U_g=0.88 m/s, μ_{fric}=0.6).

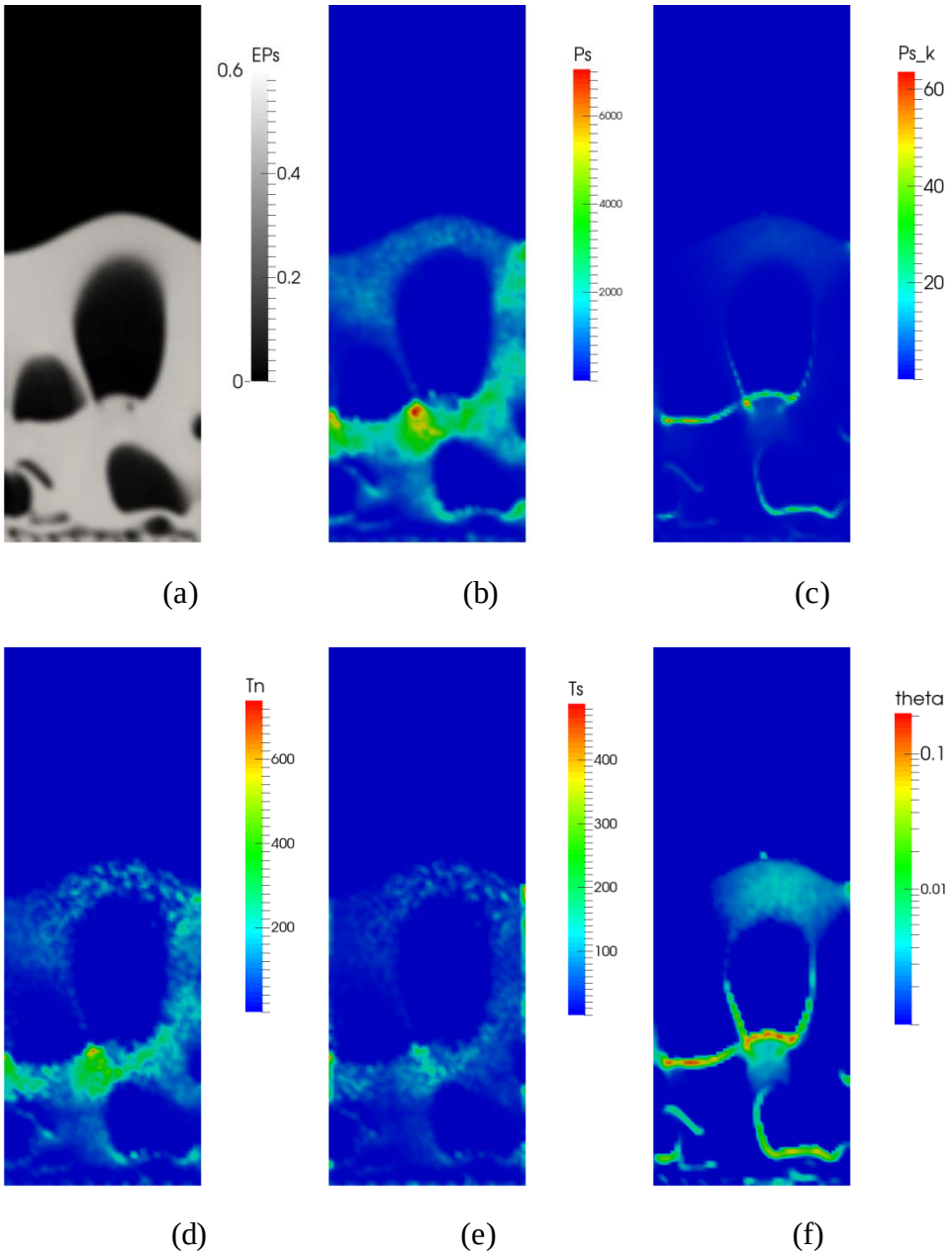

Fig. 3. Snapshots of different field variables (a) solids concentration, (b) solids pressure, (c) kinetic contribution to the solids pressure, (d) normal wall stress, (e) tangential wall stress, (f) granular temperature. (Numerical simulation: U_g=0.88m/s, μ_{fric}=0.6).

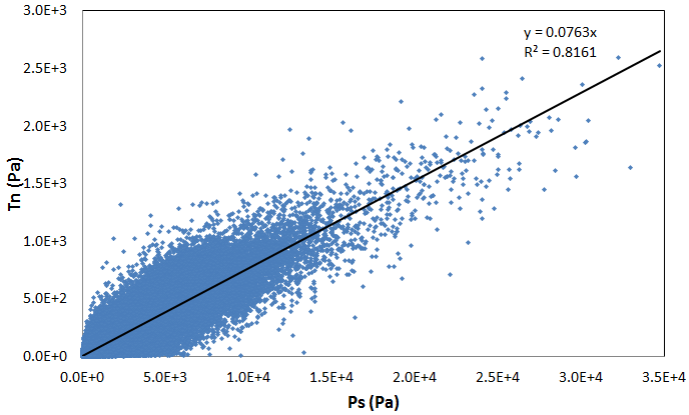

Fig. 4. Raw data of normal wall stress versus solids pressure for the emulsion phase together with a linear regression (Numerical simulation: U_g=0.88m/s, μ_{fric}=0.6).

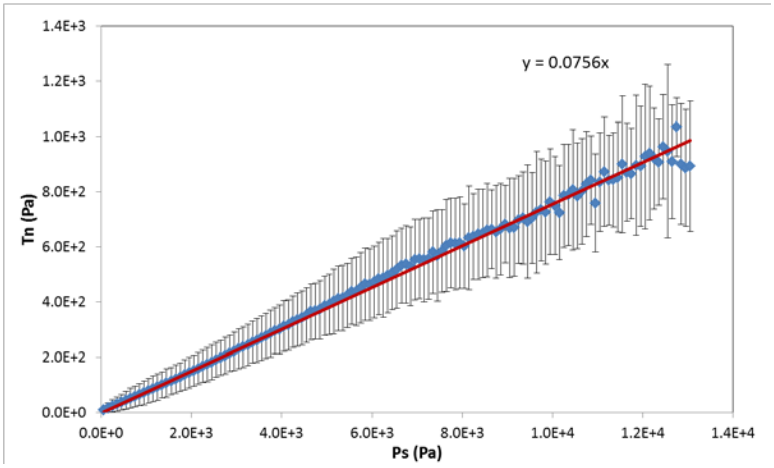

Fig. 5. Averaged normal wall stress versus solids pressure for the emulsion phase (the symbols are average data and error bars representing ± one standard deviation; Numerical simulation: U_g=0.88m/s, μ_{fric}=0.6).

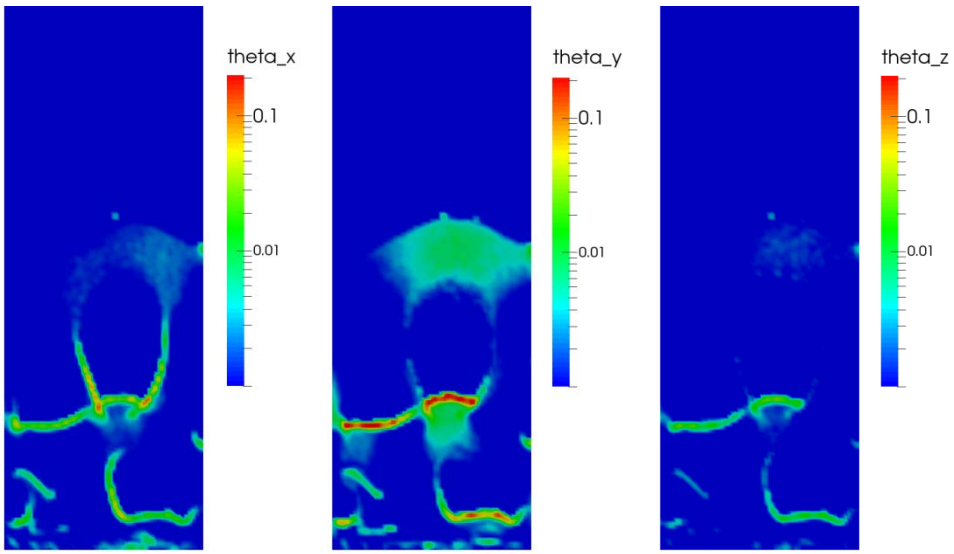

(a) (b) (c)

Fig. 6. Components of granular temperature in (a) x, (b) y and (c) z directions.

(Numerical simulation: U_g=0.88m/s, μ_{fric}=0.6).

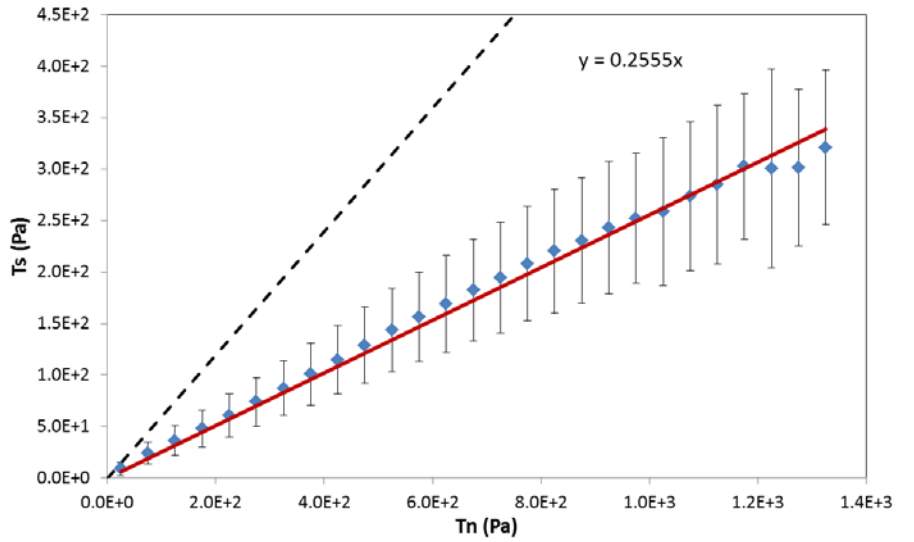

Fig. 7. Averaged tangential wall stress versus normal wall stress for the emulsion phase (the symbols are average data and error bars representing ± one standard deviation; the solid line is liner fitting; the dashed line represent equation (8) with the slope of physical particle-wall friction coefficient, Numerical simulation: U_g=0.88m/s, μ_{fric}=0.6).

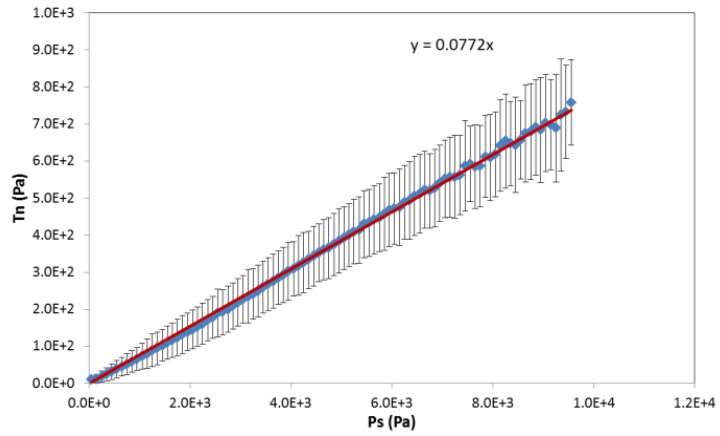
y = 0.0772x
Tn (Pa)
Ps (Pa)
1.0E+3
9.0E+2
8.0E+2
7.0E+2
6.0E+2
5.0E+2
4.0E+2
3.0E+2
2.0E+2
1.0E+2
0.0E+0
0.0E+0
2.0E+3
4.0E+3
6.0E+3
8.0E+3
1.0E+4
1.2E+4

(a)

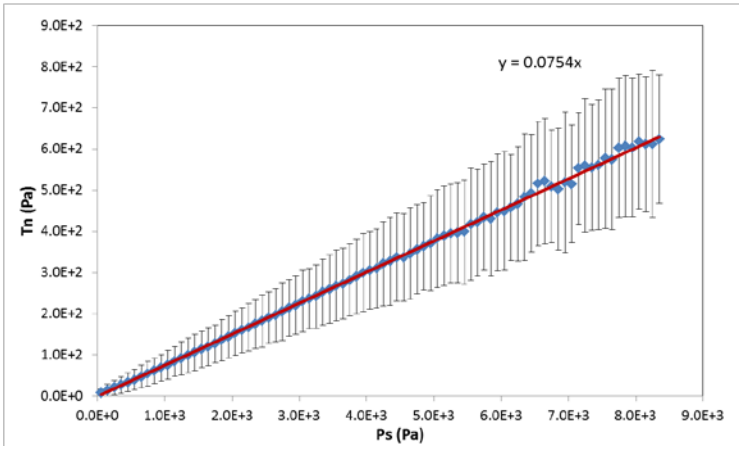
y = 0.0754x
Tn (Pa)
Ps (Pa)
9.0E+2
8.0E+2
7.0E+2
6.0E+2
5.0E+2
4.0E+2
3.0E+2
2.0E+2
1.0E+2
0.0E+0
0.0E+0
1.0E+3
2.0E+3
3.0E+3
4.0E+3
5.0E+3
6.0E+3
7.0E+3
8.0E+3
9.0E+3

(b)

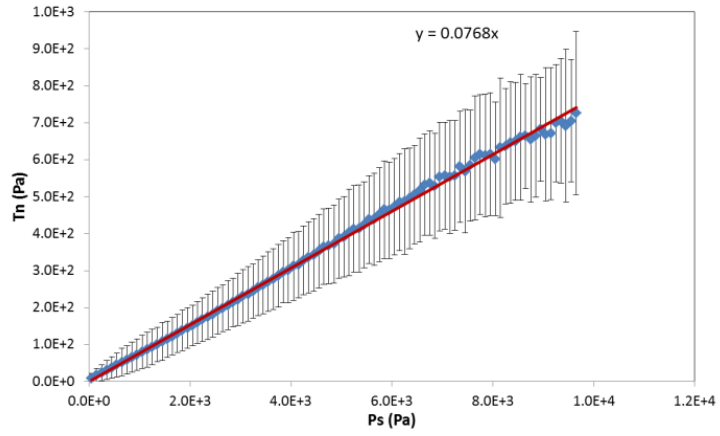
y = 0.0768x
Tn (Pa)
Ps (Pa)
1.0E+3
9.0E+2
8.0E+2
7.0E+2
6.0E+2
5.0E+2
4.0E+2
3.0E+2
2.0E+2
1.0E+2
0.0E+0
0.0E+0
2.0E+3
4.0E+3
6.0E+3
8.0E+3
1.0E+4
1.2E+4

(c)

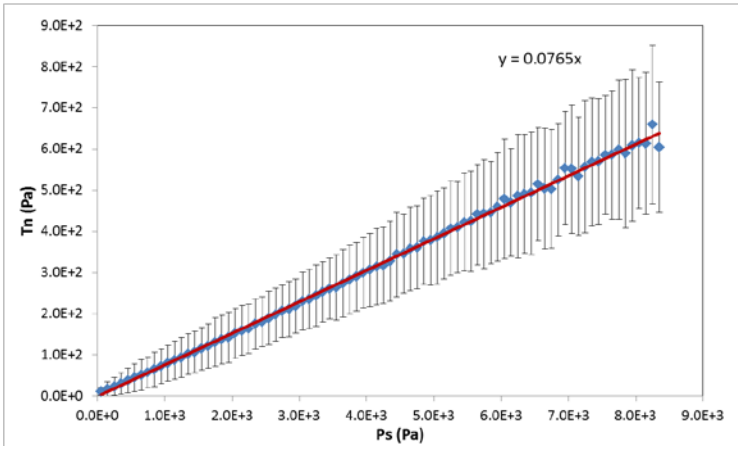

(d)

Fig. 8. Averaged normal wall stress versus solids pressure for the emulsion phase for different friction coefficients (a) μ_{fric}=0.3; (b) μ_{fric}=0.4; (c) μ_{fric}=0.5; (d) μ_{fric}=0.7.

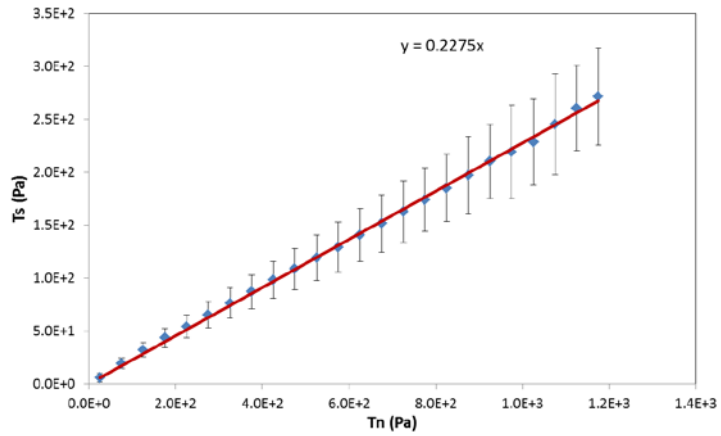
y = 0.2275x
Ts (Pa)
Tn (Pa)
3.5E+2
3.0E+2
2.5E+2
2.0E+2
1.5E+2
1.0E+2
5.0E+1
0.0E+0
0.0E+0
2.0E+2
4.0E+2
6.0E+2
8.0E+2
1.0E+3
1.2E+3
1.4E+3

(a)

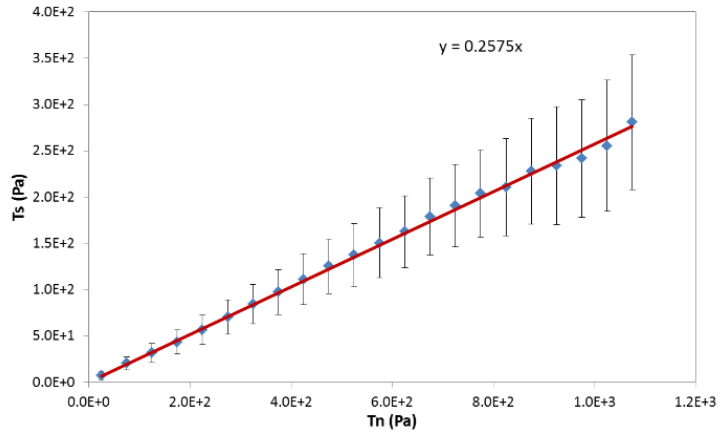
y = 0.2575x
Ts (Pa)
Tn (Pa)
4.0E+2
3.5E+2
3.0E+2
2.5E+2
2.0E+2
1.5E+2
1.0E+2
5.0E+1
0.0E+0
0.0E+0
2.0E+2
4.0E+2
6.0E+2
8.0E+2
1.0E+3
1.2E+3

(b)

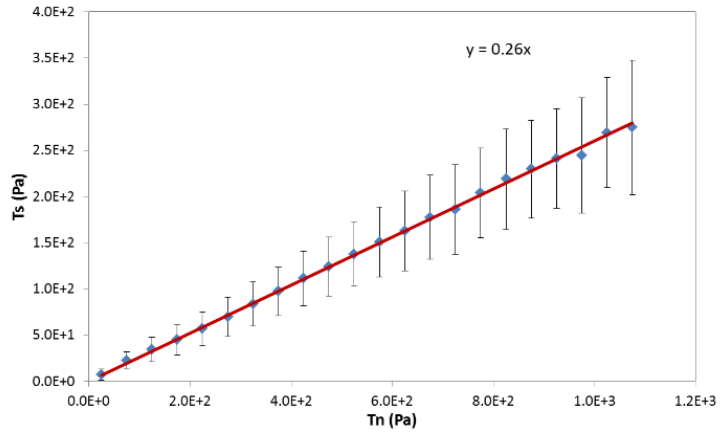
y = 0.26x
Ts (Pa)
Tn (Pa)
4.0E+2
3.5E+2
3.0E+2
2.5E+2
2.0E+2
1.5E+2
1.0E+2
5.0E+1
0.0E+0
0.0E+0
2.0E+2
4.0E+2
6.0E+2
8.0E+2
1.0E+3
1.2E+3

(c)

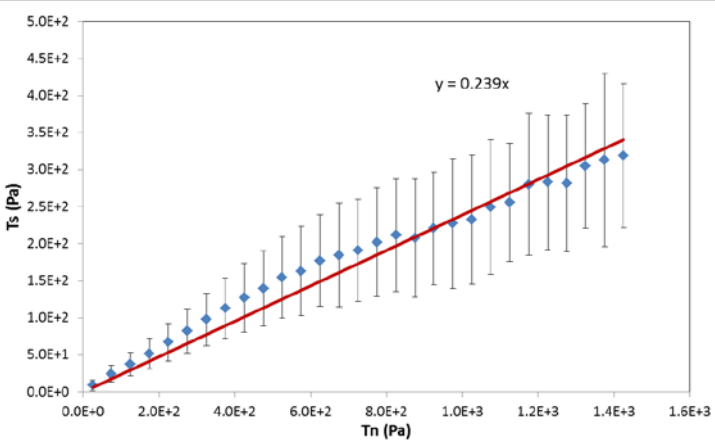

(d)

Fig. 9. Averaged tangential wall stress versus normal wall stress for the emulsion phase for different friction coefficients (a) μ_{fric}=0.3; (b) μ_{fric}=0.4; (c) μ_{fric}=0.5; (d) μ_{fric}=0.7.

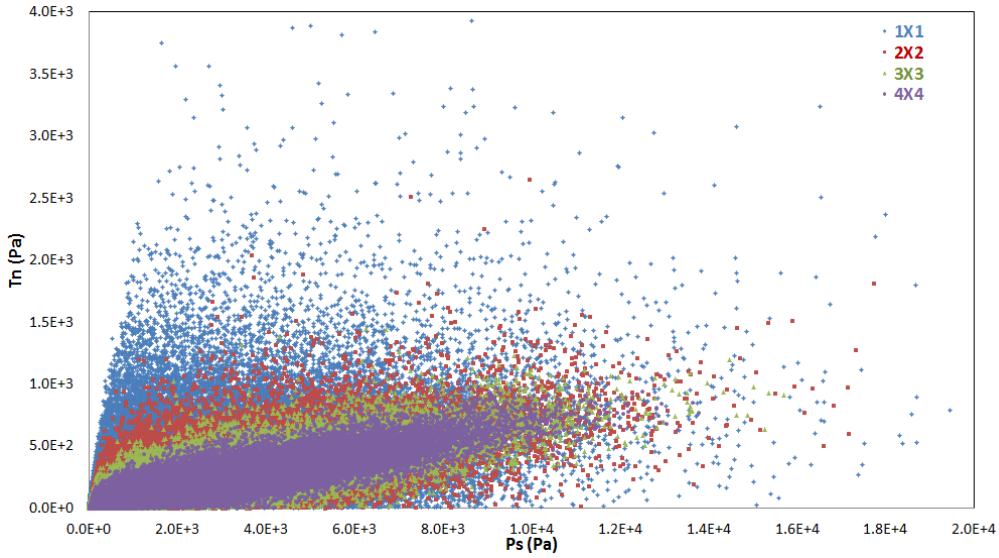

Fig. 10. Normal wall stress versus solids pressure in the emulsion phase for the simulation with spring constant of 200000 N/m using different window sizes (Numerical simulation: U_g=0.88m/s, μ_{fric}=0.6).

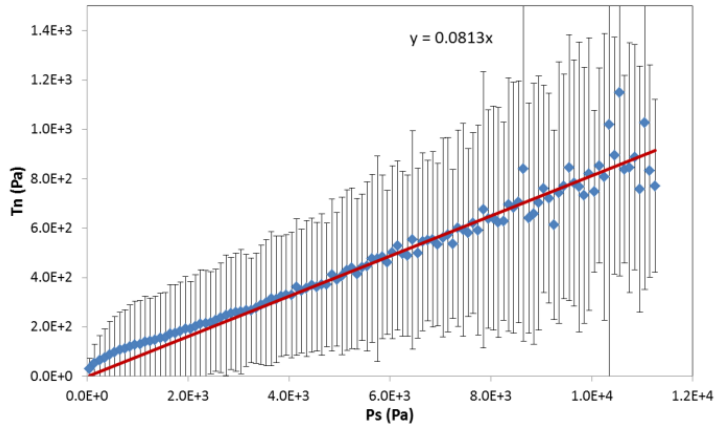
y = 0.0813x
Tn (Pa)
Ps (Pa)
1.4E+3
1.2E+3
1.0E+3
8.0E+2
6.0E+2
4.0E+2
2.0E+2
0.0E+0
0.0E+0
2.0E+3
4.0E+3
6.0E+3
8.0E+3
1.0E+4
1.2E+4

(a)

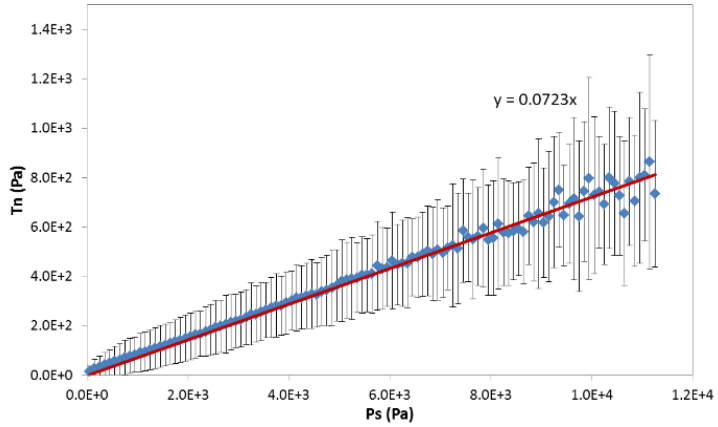
y = 0.0723x
Tn (Pa)
Ps (Pa)
1.4E+3
1.2E+3
1.0E+3
8.0E+2
6.0E+2
4.0E+2
2.0E+2
0.0E+0
0.0E+0
2.0E+3
4.0E+3
6.0E+3
8.0E+3
1.0E+4
1.2E+4

(b)

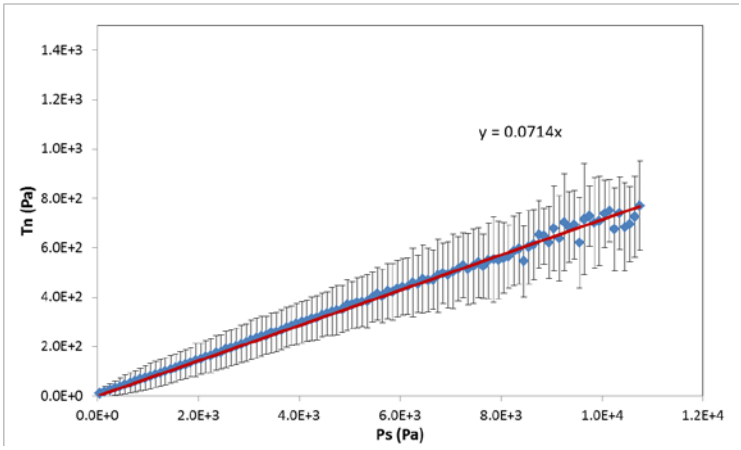
y = 0.0714x
Tn (Pa)
Ps (Pa)
1.4E+3
1.2E+3
1.0E+3
8.0E+2
6.0E+2
4.0E+2
2.0E+2
0.0E+0
0.0E+0
2.0E+3
4.0E+3
6.0E+3
8.0E+3
1.0E+4
1.2E+4

(c)

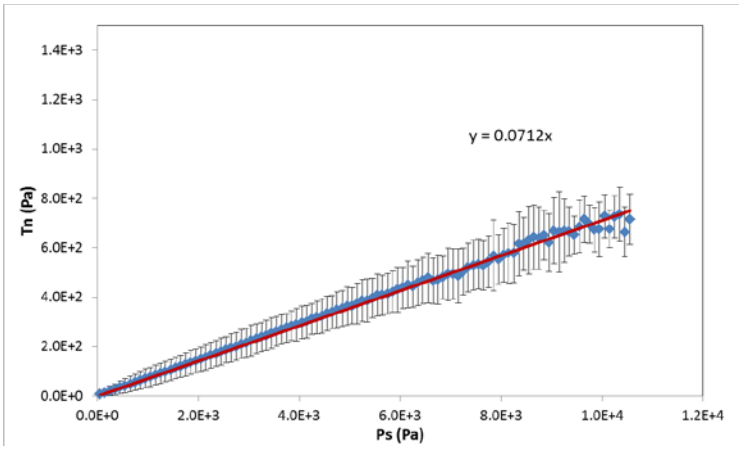

(d)

Fig. 11. Averaged normal wall stress versus solids pressure in the emulsion phase for the simulation with spring constant of 200000 N/m using different window sizes (a) 1×1, (b) 2×2, (c) 3×3, (d) 4×4 (Numerical simulation: U_g=0.88m/s, μ_{fric}=0.6).

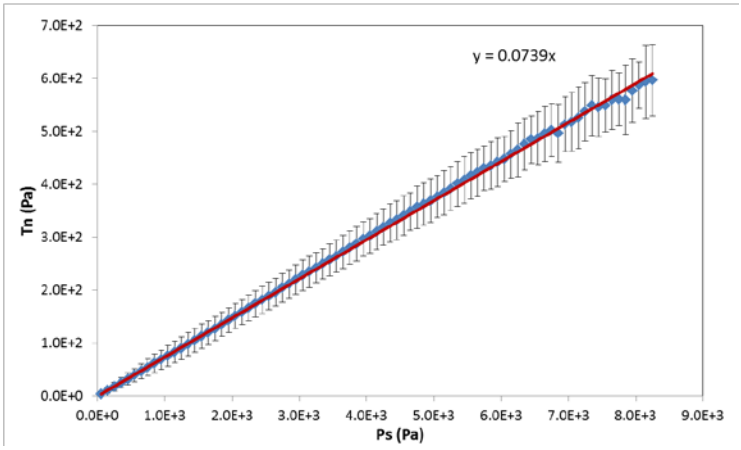
y = 0.0739x
Tn (Pa)
Ps (Pa)
7.0E+2
6.0E+2
5.0E+2
4.0E+2
3.0E+2
2.0E+2
1.0E+2
0.0E+0
0.0E+0
1.0E+3
2.0E+3
3.0E+3
4.0E+3
5.0E+3
6.0E+3
7.0E+3
8.0E+3
9.0E+3

(a)

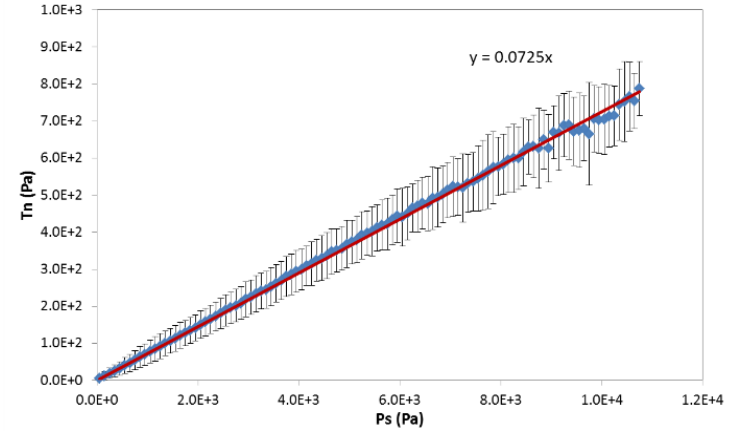
y = 0.0725x
Tn (Pa)
Ps (Pa)
1.0E+3
9.0E+2
8.0E+2
7.0E+2
6.0E+2
5.0E+2
4.0E+2
3.0E+2
2.0E+2
1.0E+2
0.0E+0
0.0E+0
2.0E+3
4.0E+3
6.0E+3
8.0E+3
1.0E+4
1.2E+4

(b)

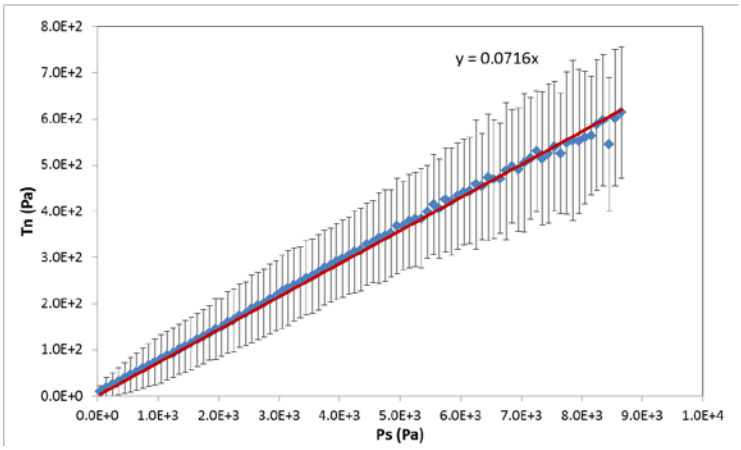
y = 0.0716x
Tn (Pa)
Ps (Pa)
8.0E+2
7.0E+2
6.0E+2
5.0E+2
4.0E+2
3.0E+2
2.0E+2
1.0E+2
0.0E+0
0.0E+0
1.0E+3
2.0E+3
3.0E+3
4.0E+3
5.0E+3
6.0E+3
7.0E+3
8.0E+3
9.0E+3
1.0E+4

(c)

Fig. 12. Normal wall stress versus solids pressure for the emulsion phase together with a linear regression for different spring constant (a) 2000 N/m; (b) 20000 N/m; (c) 200000 N/m (Numerical simulation: U_g=0.88m/s, μ_{fric}=0.6).

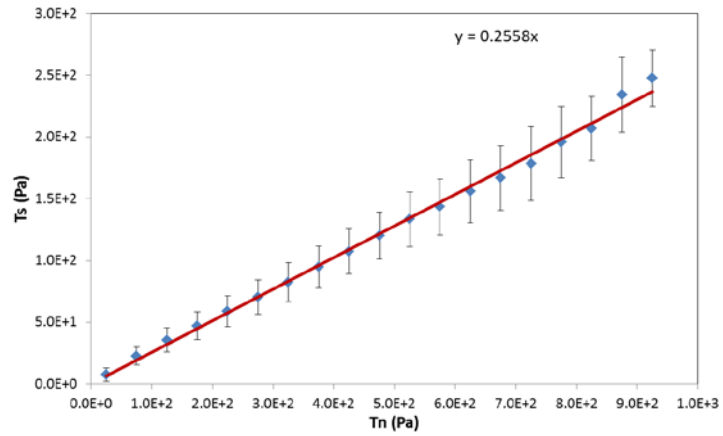
y = 0.2558x
Ts (Pa)
Tn (Pa)
3.0E+2
2.5E+2
2.0E+2
1.5E+2
1.0E+2
5.0E+1
0.0E+0
0.0E+0
1.0E+2
2.0E+2
3.0E+2
4.0E+2
5.0E+2
6.0E+2
7.0E+2
8.0E+2
9.0E+2
1.0E+3

(a)

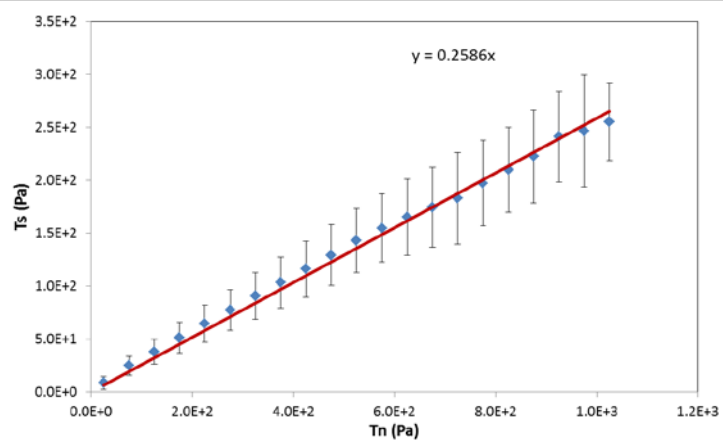
y = 0.2586x
Ts (Pa)
Tn (Pa)
3.5E+2
3.0E+2
2.5E+2
2.0E+2
1.5E+2
1.0E+2
5.0E+1
0.0E+0
0.0E+0
2.0E+2
4.0E+2
6.0E+2
8.0E+2
1.0E+3
1.2E+3

(b)

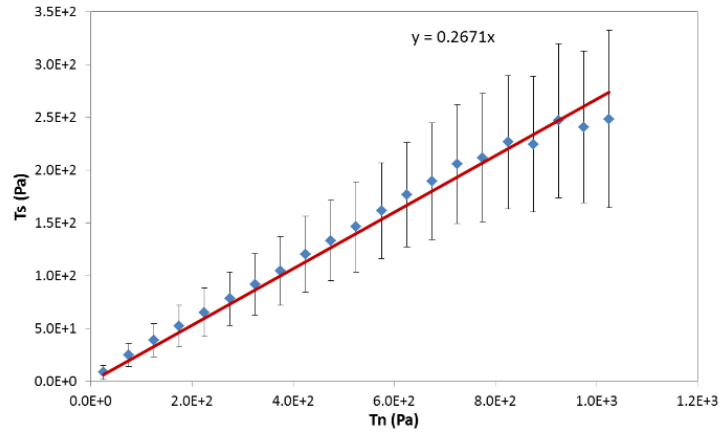
y = 0.2671x
Ts (Pa)
Tn (Pa)
3.5E+2
3.0E+2
2.5E+2
2.0E+2
1.5E+2
1.0E+2
5.0E+1
0.0E+0
0.0E+0
2.0E+2
4.0E+2
6.0E+2
8.0E+2
1.0E+3
1.2E+3

(c)

Fig. 13. Tangential wall stress versus normal wall stress for the emulsion phase together with a linear regression for different spring constant (a) 2000 N/m; (b) 20000 N/m; (c) 200000 N/m (Numerical simulation: U_g=0.88m/s, μ_{fric}=0.6).

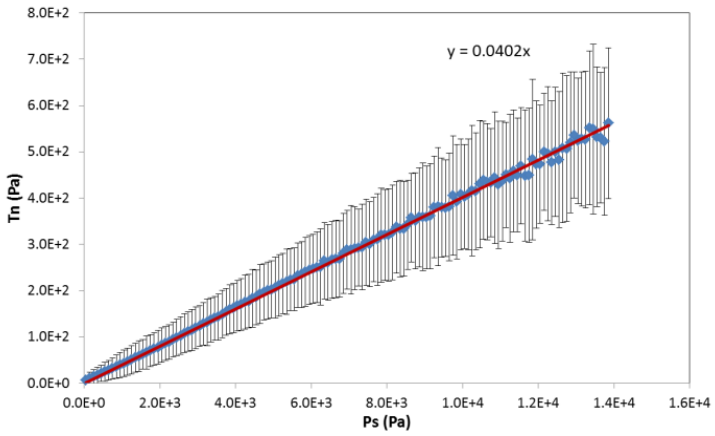

(a)

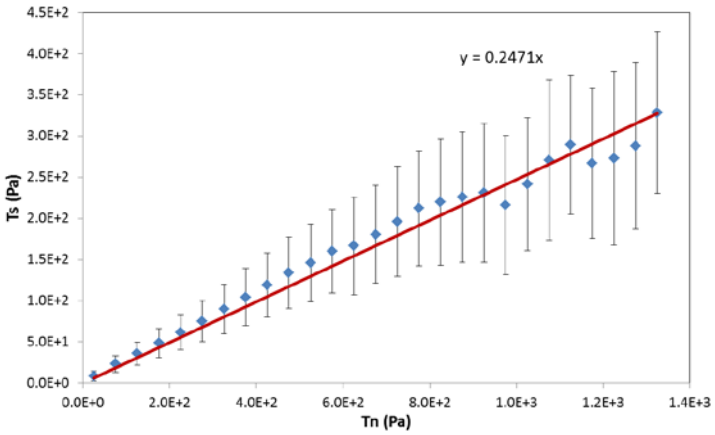

(b)

Fig. 14. Results predicted by 2.5 mm grid in the thickness direction (a) Normal wall stress versus solids pressure; (b) Tangential wall stress versus normal wall stress (Numerical simulation: U_g=0.88m/s, μ_{fric}=0.6).

Table 1. Equations and closure models solved in MFIX-DEM for the current study

Gas phase
$\frac{\partial(\varepsilon_g \rho_g)}{\partial t} + \nabla \cdot (\varepsilon_g \rho_g \mathbf{v}_g) = 0$ $\frac{d}{dt}\left(\varepsilon_g \rho_g \mathbf{v}_g\right) = \nabla \cdot \bar{\bar{S}}_g + \varepsilon_g \rho_g \mathbf{g} - \mathbf{I}_{gs}$ $\bar{\bar{S}}_g = -P_g \bar{\bar{I}} + \bar{\bar{\tau}}_g$
DEM Particle
$\frac{d\mathbf{x}_i}{dt} = \mathbf{u}_i$ $m_i \frac{d\mathbf{v}_i}{dt} = \mathbf{F}_i$ $I_i \frac{d\boldsymbol{\omega}_i}{dt} = \mathbf{T}_i$
Closures
$\varepsilon_s + \varepsilon_g = 1$ $\mathbf{F}_i = m_i \mathbf{g} + \mathbf{F}_i^c + \mathbf{F}_i^d$ $\mathbf{F}_i^c$ closed by the soft sphere model (Cundall and Strack 1979) $\mathbf{F}_i^d = -\nabla P_g(\mathbf{x}_i) V_i + \frac{\beta_i V_i}{\varepsilon_s}\left(\mathbf{v}_g(\mathbf{x}_i) - \mathbf{u}_i\right)$ $\mathbf{I}_{gs} = \frac{1}{V}\sum_{i=1}^{N} \mathbf{F}_i^d$ $\beta_i = \begin{cases} 150\frac{\varepsilon_s(1-\varepsilon_g)\mu_g}{\varepsilon_g d_i^2} + 1.75\frac{\varepsilon_s \rho_g \left\|\mathbf{v}_g(\mathbf{x}_i) - \mathbf{u}_i\right\|}{d_i} & \text{if } \varepsilon_g < 0.8 \\ \frac{3}{4} C_{D,i} \varepsilon_g^{-2.65} \frac{\varepsilon_s \varepsilon_g \rho_g \left\|\mathbf{v}_g(\mathbf{x}_i) - \mathbf{u}_i\right\|}{d_i} & \text{if } \varepsilon_g \geq 0.8 \end{cases}$

$$C_{D,i} = \begin{cases} \dfrac{24}{\mathrm{Re}_i \cdot \varepsilon_g}(1 + 0.15(\mathrm{Re}_i \cdot \varepsilon_g)^{0.687}) & \text{if } \mathrm{Re}_i \cdot \varepsilon_g < 1000 \\ 0.44 & \text{if } \mathrm{Re}_i \cdot \varepsilon_g \geq 1000 \end{cases}$$

$$\mathrm{Re}_i = \frac{\rho_g \left| \mathbf{v}_g(\mathbf{x}_i) - \mathbf{u}_i \right| d_i}{\mu_g}$$

Table 2. Parameters used in the baseline numerical simulation.

Parameter	**Value**	**Parameter**	**Value**
Bed height, (m)	1	Bed width, (m)	0.3
Bed thickness, (m)	0.01	Static bed height, (m)	0.3
Particles density, (kg/m^3)	2500	Particle diameter, (mm)	0.7
Gas density, (kg/m^3)	1.2	Pressure, (atm)	1
Normal inter-particle spring constant, (N/m)	2000	Tangential inter-particle spring constant, (N/m)	571
Inter-particle restitution coefficient, (-)	0.95	Particle-particle frictional coefficient, (-)	0.6
Normal wall-particle spring constant, (N/m)	2000	Tangential wall-particle spring constant, (N/m)	571
Particle-wall restitution coefficient, (-)	0.8	Particle-wall frictional coefficient, (-)	0.6
Superficial gas velocity, (m/s)	0.88	Numerical grid size, (mm)	5